

****Volume Title****

ASP Conference Series, Vol. **Volume Number**

****Author****

© **Copyright Year Astronomical Society of the Pacific**

Diagnosing small- and large-scale structure in the winds of hot, massive OB-stars

J.O. Sundqvist,¹ & S.P. Owocki,¹

¹*Dept. of Physics & Astronomy, University of Delaware, USA*

Abstract.

It is observationally as well as theoretically well established that the winds of hot, massive OB-stars are highly structured on a broad range of spatial scales. This paper first discusses consequences of the *small-scale* structures associated with the strong instability inherent to the line-driving of these winds. We demonstrate the importance of a proper treatment of such wind clumping to obtain reliable estimates of mass-loss rates, and also show that instability simulations that are perturbed at the lower boundary indeed display significant clumping quite close to the wind base, in general agreement with observations.

But a growing subset of massive stars has also been found to possess strong surface magnetic fields, which may channel the star's outflow and induce also *large-scale* wind structures and cyclic behavior of spectral diagnostics. The paper concludes by showing that multi-dimensional, magneto-hydrodynamical wind simulations, together with detailed radiative-transfer modeling, can reproduce remarkably well the periodic Balmer line emission observed in slowly rotating magnetic O stars like HD 191612.

1. Introduction

Hot, massive OB-stars have strong winds, with typical mass-loss rates $\dot{M} \approx 10^{-6} M_{\odot}/\text{yr}$ and terminal speeds $v_{\infty} \approx 2000 \text{ km/s}$, driven by metal-line scattering of the star's intense continuum radiation field. The first quantitative description of such line-driving was given in the seminal paper by (Castor et al. 1975, CAK), who assumed a steady-state, spherically symmetric, and homogeneous outflow. And since then, extensions and applications of this CAK theory have had considerable success in explaining many of the observed gross properties and global trends of hot star winds, such as the relation between the wind momentum and the stellar luminosity and the basic metallicity dependence of mass-loss rates. Nevertheless, it has over the years also become very clear that, actually, these winds are neither steady-state, nor homogeneous; rather they seem to be highly structured on a broad range of spatial scales. (For a very comprehensive review of hot star winds, we refer the reader to Puls et al. 2008.)

This paper summarizes our ongoing efforts in characterizing the nature and consequences of such wind structure. After first briefly reviewing the background to the strong instability inherent to line driving, we next concentrate on confronting theoretical predictions of the resulting *small-scale* structure with observations, and examine what consequences such wind clumping have for the interpretation of spectral diagnostics. The paper then continues by discussing how the presence of a strong surface magnetic field may channel the outflow along closed field lines, and how the *large-scale*

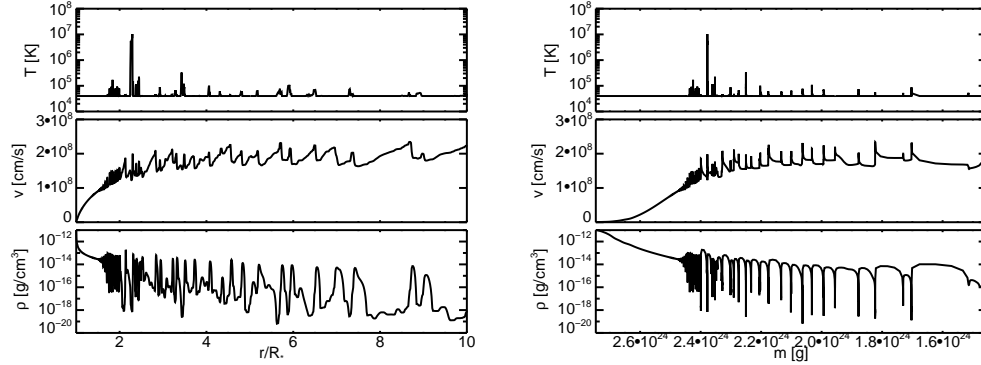


Figure 1. Snapshot of temperature, velocity, and density in a 1-D LDI simulation, plotted versus radius (left) and a Lagrangian mass coordinate (right), as defined in e.g. Owocki et al. (1988) and illustrating how little wind mass is contained in the high-speed rarefactions.

wind structures predicted by simulations of such magnetically confined winds may be diagnosed using the rotational phase variation of optical recombination lines like $H\alpha$.

2. Small-scale structure and wind clumping

The amount of evidence supporting a clumped stellar wind is nowadays overwhelming. Sundqvist et al. (2011a) give a comprehensive overview of the current status; this paper concentrates on two items, namely i) the theoretical background and ii) the effects of clumping on wind diagnostics used to derive mass-loss rates and clumping properties.

2.1. Theory: The line-deshadowing instability

Linear stability analyses showed already during the 80s (Owocki & Rybicki 1984, 1985) that the line force responsible for accelerating hot star winds is highly unstable on spatial scales near and below the Sobolev length $L = v_{\text{th}}/(dv/dr) \approx (v_{\text{th}}/v)r \approx 0.01r$, where $v_{\text{th}} \approx 10$ km/s is the ion thermal speed and $v \approx 1000$ km/s is a typical wind flow speed. Direct numerical modeling (Owocki et al. 1988; Feldmeier 1995; Dessart & Owocki 2005) has since confirmed that the non-linear growth of this *line-deshadowing instability* (LDI) leads to high speed rarefactions that steepen into strong reverse shocks, whereby most wind material is compressed into spatially very narrow “clumps” (or shells in 1-D simulations). Fig. 1 illustrates this characteristic structure, which forms the basis for our current understanding and interpretation of wind clumping. Further, the presence of strong shocks and hot gas in LDI simulations also provide a generally accepted explanation for the soft X-rays observed from OB-stars by orbiting telescopes like CHANDRA (Feldmeier et al. 1997, see also Cohen, this volume).

The simulation snapshot displayed in Fig. 1 has been calculated using the numerical hydrodynamics code VH-1 (developed by J. Blondin et al.), with the radiation line force computed following the so-called smooth source function (SSF, Owocki & Puls 1996) approach. The SSF method allows one to follow the non-linear evolution of the LDI, while also accounting for the stabilizing line-drag effect (Lucy 1984) of the diffuse, scattered radiation field. In the displayed simulation, this line drag exactly cancels

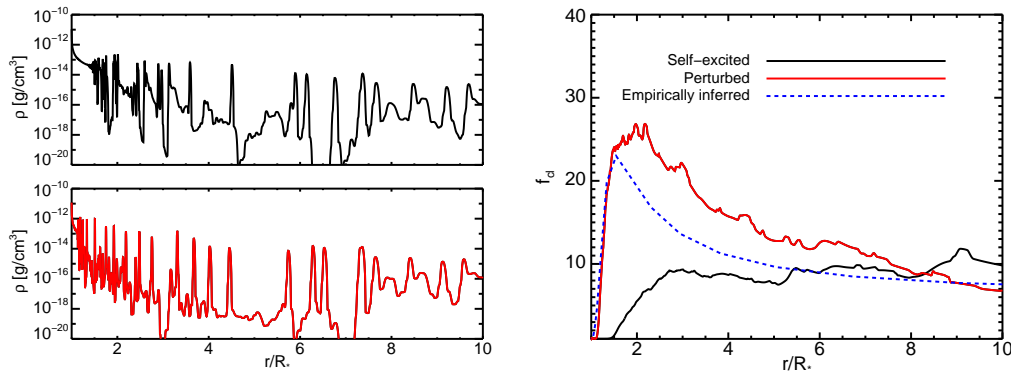


Figure 2. **Left:** Density snapshots for an LDI simulation with self-excited structure (upper) and one in which the lower boundary has been perturbed by a sound wave (lower). **Right:** Radial stratification of the clumping factor as derived for ζ Pup by Najarro et al. (2011) vs. theoretical predictions.

the LDI at the stellar surface, leading to marginal stabilization of the wind base. However, as mass parcels move away from the stellar surface, the relative influence of the line-drag decreases and structure starts to develop, roughly at $r \approx 1.5R_*$.

But note that the exact amount of such instability-damping in the lower wind depends critically on delicate details of the competition between the LDI (arising from direct absorption of stellar continuum radiation) and the line-drag (arising from the scattering source function), and so is quite sensitive to, e.g., external perturbations. Indeed, we report here on additional model computations in which we perturb the density ρ_0 at the lower boundary by introducing a generic sound wave of amplitude $\delta\rho/\rho_0 = 0.25$ and period 4000 sec. And such simulations now display significant structure much closer to the wind base, as shown by Fig. 2. The right panel of this figure compares the radial stratification of the time-averaged clumping factor $f_{cl} \equiv \langle \rho^2 \rangle / \langle \rho \rangle^2$ in simulations with self-excited structure and a perturbed lower boundary, respectively, and shows clearly how the latter model is more strongly clumped in the inner wind. This result is in general good agreement with observations, as further discussed at the end of Sect. 2.2.

2.2. Diagnostics: Deriving mass-loss rates and clumping properties of OB-star winds

The average mass-loss rate from a time-dependent LDI simulation actually is quite similar to that of its steady-state CAK start model, suggesting the resulting wind structure only has secondary effects¹ on theoretical mass-loss predictions. On the other hand, the structure in density and velocity seriously affects the radiative transfer through the wind, and thereby also the interpretation of *observed* spectra.

To illustrate this, let us compare mass-loss rates derived from different wind diagnostics using *smooth* wind models. Taking the Galactic O6 supergiant λ Cep as an example, Fig. 3 shows how the rate derived from the optical recombination line $H\alpha$ is ~ 20 times higher than the rate derived from the UV resonance lines of phosphorus v

¹from, e.g., a changed wind ionization balance (Muijres et al. 2011).

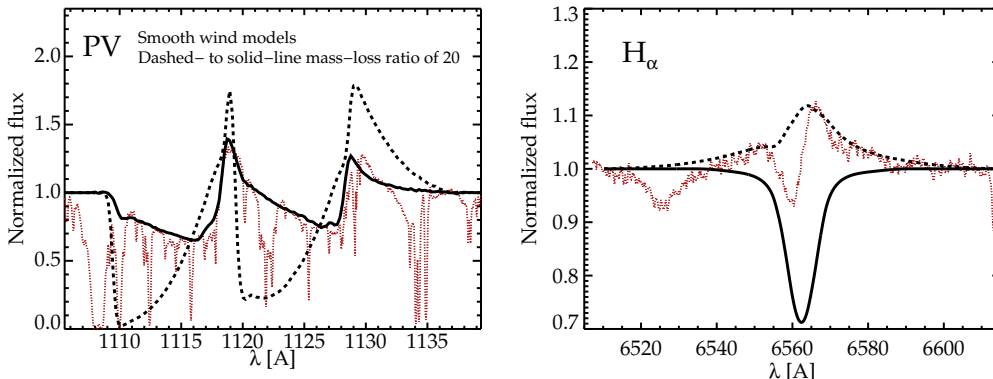


Figure 3. Observed (dotted red lines) and synthetic (black solid and dashed lines) PV and $H\alpha$ line profiles in λ Cep. Observations from Fullerton et al. (2006) and Markova et al. (2005). Synthetic profiles calculated using the unified (photosphere+wind) NLTE model atmosphere code `FASTWIND` (Puls et al. 2005) and the Monte-Carlo code developed by Sundqvist et al. (2010, 2011b). All profiles were calculated assuming a *smooth* wind, and illustrate how the mass-loss rate ($6 \times 10^{-6} M_{\odot}/\text{yr}$) required to fit $H\alpha$ is ~ 20 times higher than that required to fit the PV lines.

(PV), the latter also being almost an order of magnitude lower than predicted by the line-driven wind theory! Such inconsistencies have been found by many studies (with perhaps the most prominent example being the study of PV in 40 Galactic O stars by Fullerton et al. 2006), and are likely a consequence of neglecting wind clumping when deriving the mass-loss rates.

Most diagnostic studies of clumping have assumed that the wind consists of statistically distributed, *optically thin* clumps embedded in a void background medium, and neglected any disturbances on the velocity field. The most important result of such optically thin clumping is that the opacities of diagnostics depending on the square of the density, such as $H\alpha$ and thermal infra-red/radio emission, are higher than in a smooth wind model with the same mass-loss rate. The scaling invariant is $\sqrt{f_{\text{cl}}}\dot{M}$, leading to overestimates of mass-loss rates derived from smooth wind models by $\sqrt{f_{\text{cl}}}$. In contrast, diagnostics depending only linearly on density, such as UV resonance lines and bound-free attenuation of X-rays, are not directly affected by optically thin clumping². Combined optical/infra-red/radio studies (Puls et al. 2006; Najarro et al. 2011) using this approach typically show that mass-loss rates derived from $H\alpha$ and smooth wind models should be scaled down by factors 2...5. Such reductions have also been confirmed by independent studies of bound-free X-ray attenuation (Cohen et al. 2010, 2011, see also Cohen, this volume), and would imply modest reductions of present-day theoretical predictions of mass-loss rates, as well as clumping factors on order $f_{\text{cl}} \approx 10$.

Clumping in the inner wind. While such characteristic clumping factors are in general accordance with theoretical predictions, diagnostic studies (Eversberg et al. 1998; Bouret et al. 2003; Puls et al. 2006; Cohen et al. 2011) also suggest the wind is sig-

²they can be indirectly affected though, through a modified ionization balance (e.g. Bouret et al. 2003)

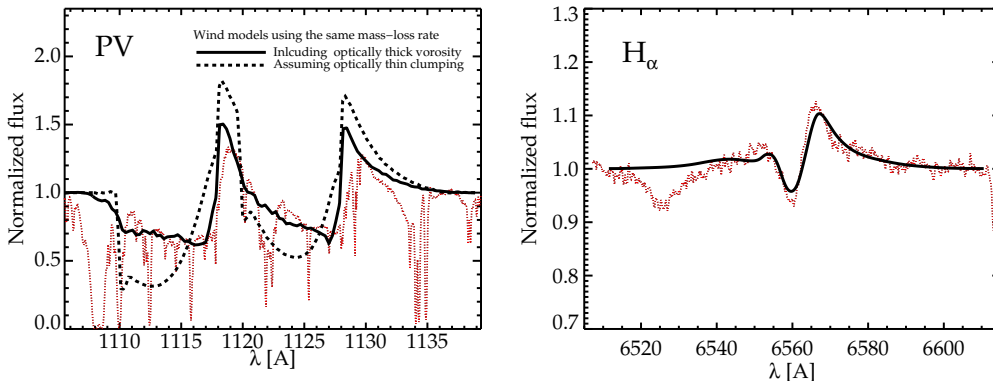


Figure 4. Same as Fig. 3, but now accounting for clumping and optically thick vorosity (solid lines, see text), and using a single mass-loss rate $1.5 \times 10^{-6} M_{\odot}/\text{yr}$. As an illustration of the importance of optically thick clumping for UV resonance lines, the dashed lines show synthetic PV profiles calculated with the same mass-loss rate but now under the assumption of *optically thin* clumps (i.e. neglecting vorosity).

nificantly structured well below the $r \approx 1.5R_{\star}$ predicted for the onset of clumping by standard LDI simulations with self-excited structure. The right panel of Fig. 2 compares the radial stratification of f_{cl} derived for ζ Pup by the comprehensive multi-diagnostic study by Najarro et al. (2011) with theoretical predictions. The figure shows that perturbing the lower boundary (see Sect. 2.1) can indeed induce significant wind structure also in the lower wind, leading then to quite good overall agreement with observations. A journal paper discussing such base perturbations, as well as other effects that may affect the predicted structure in the inner wind, is currently in preparation.

Optically thick clumping – porosity and vorosity. But note that such optically thin clumping does not really help explain the unexpected weakness of the PV lines displayed in Fig. 4, as these line are basically unaffected by this approach. It is important to realize, however, that if the assertion of optically thin clumps is not met for the investigated process, additional effects become important in the radiative transfer. For continuum diagnostics, self-shielding of opacity within optically thick clumps leads to increased escape of photons through porous channels in between the clumps. Such *porosity* thus has the general effect of reducing the wind’s effective opacity (Feldmeier et al. 2003; Owocki et al. 2004). Though it has been suggested porosity might be important for X-ray line attenuation in hot star winds (Feldmeier et al. 2003; Oskinova et al. 2006), recent studies show that this is quite unlikely as there is no apparent evidence for significant porosity in the data (Cohen et al. 2008, Leutenegger et al., submitted) and it would further imply mean free paths between clumps much longer than predicted by theory (Owocki & Cohen 2006; Sundqvist et al. 2012a).

But the situation is quite different for the inherently very strong UV resonance *lines*, in which clumps easily can become optically thick (Oskinova et al. 2007). Due to the narrow Doppler width of the line profile, line photons in a rapidly expanding stellar wind can only interact with the plasma over a very narrow spatial range. Therefore many such line photons will simply leak through the wind via “porous” channels in the velocity field, without ever interacting with the optically thick clumps. Hence this

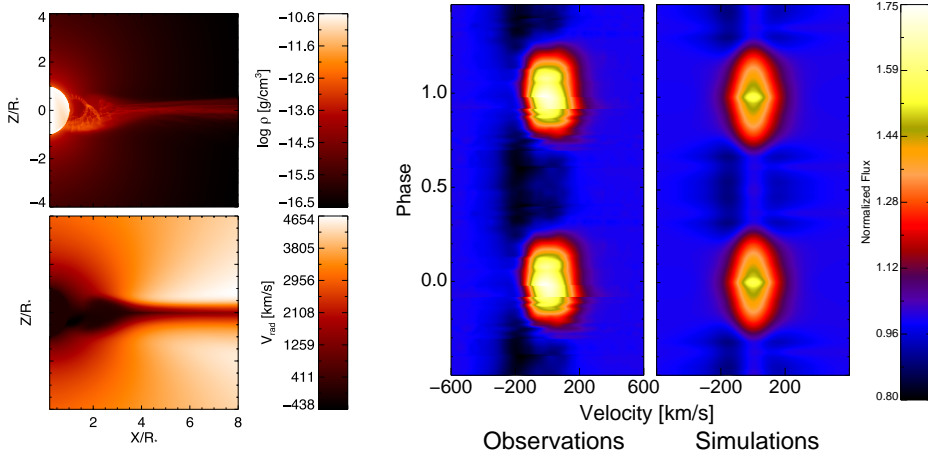


Figure 5. **Left:** Contour maps of density (upper) and radial velocity (lower) in an MHD wind simulation, obtained by averaging over ~ 100 snapshots well after initiation. **Right:** Observed (ephemeris from Howarth et al. 2007) and synthetic $H\alpha$ dynamic spectra for HD19162, calculated as described in the text and in Sundqvist et al. (2012b).

effect has been dubbed velocity porosity, or “vorosity” (Owocki 2008). And in analogy with spatial porosity, the main effect of such vorosity is to reduce the wind’s effective opacity.

Using models accounting for both clumping and optically thick vorosity, Fig. 4 again shows PV and $H\alpha$ fits to λ Cep. And in contrast to before (Fig. 3), both diagnostics can now be well fit using the same mass-loss rate, which now is only a modest factor of two lower than the theoretical prediction by Vink et al. (2000). This illustrates the importance of a proper treatment of wind clumping when deriving mass-loss rates from OB-stars.

3. Large-scale wind structure due to magnetic fields

Let us now switch focus from the small-scale structures associated with the LDI to the more large-scale wind structures associated with the presence of a strong surface magnetic field. Due to recent advances in spectropolarimetric techniques, such large-scale fields are being detected in OB-stars at an increasing rate (for an overview of the current observational status, see e.g. Wade, this volume).

3.1. Theory: Dynamical magnetospheres

The effectiveness of the magnetic field in channeling the stellar wind outflow may be characterized by the ratio of the magnetic to wind kinetic energy density:

$$\eta = \frac{B^2/(8\pi)}{\rho v^2/2} = \eta_\star \frac{(r/R_\star)^{-4}}{v/v_\infty}, \quad (1)$$

where the second equality assumes a dipolar field and defines the so-called wind confinement parameter $\eta_\star = (B_\star^2 R_\star^2)/(\dot{M} v_\infty)$ (ud-Doula & Owocki 2002), with B_\star the

equatorial surface field strength. A key point is that for $\eta_\star > 1$, the Alfvén radius $R_A \approx \eta_\star^{1/4} R_\star$ at which the magnetic and wind kinetic energy densities are equal is located away from the stellar surface, allowing then for wind plasma to be channeled along closed field loops toward the magnetic equator. But note also that the steeper radial decline of the magnetic energy density than the wind kinetic energy density inevitably means the wind will always dominate at large enough radii (as is directly evident from the second equality in eqn. 1) and force the field lines to open up and essentially follow the radial flow.

Magneto-hydrodynamical (MHD) simulations following the time-evolution of the competition between the magnetic field and the radiatively driven wind confirms this basic picture (ud-Doula & Owocki 2002). The MHD simulation (computed by A. ud-Doula) used to synthesize the $H\alpha$ emission in the following section is described in Sundqvist et al. (2012b) and assumes $\eta_\star = 50$. The left panels of Fig. 5 show that below the Alfvén radius $R_A \approx 2.7R_\star$ the wind indeed becomes trapped and the material is pulled back onto the star by gravity. But despite this very dynamic behavior, with gas constantly in upward and downward motion, the transient suspension of plasma within such closed field loops leads to a region around the magnetic equator that statistically is overdense.

Note that this structure is physically distinct from that predicted for rapidly rotating magnetic stars characterized by $R_A > R_K$ (Townsend & Owocki 2005; ud-Doula et al. 2008), where R_K is the Kepler corotation radius at which the centrifugal force balances gravity. For such stars, centrifugal forces can support any trapped material above R_K , which allows for accumulation of wind plasma over very long time-scales and to the formation of a *centrifugal magnetosphere* (CM). In contrast, the characteristic structure described above, appropriate for slowly rotating magnetic stars with $R_\star < R_A < R_K$, forms a *dynamical magnetosphere* (DM). An important distinction between a CM and a DM is that the latter accumulates wind plasma only over the relatively short dynamical time-scale, implying that such DMs require the quite high mass-loss feeding rate of an O star in order to emit in $H\alpha$ (Sundqvist et al. 2012b, see also Petit & Owocki, in prep.).

3.2. Diagnostics: Rotational phase variation of Balmer line emission

We compute synthetic $H\alpha$ profiles directly from the MHD simulation discussed above by solving the formal integral of the radiative transfer equation in a 3-D cylindrical coordinate system aligned toward the observer. Since we target slowly rotating stars, we may neglect rotational effects on the wind dynamics and use the same simulation for any obliquity angle β between the rotation and magnetic axes. Sundqvist et al. (2012b) give a full description of the computation method. The right panel of Fig. 5 compares the rotational phase variation of such synthetic $H\alpha$ spectra with observations of the very slowly rotating ($P = 538$ days, $v_{\text{rot}} \approx 1$ km/s, Howarth et al. 2007) magnetic O star HD 191612, using an inclination angle $i = 50^\circ$ and $\beta = 50^\circ$, consistent with the magnetic geometry constraints derived by Wade et al. (2011). Fig. 5 shows that both the peak flux at phase 0 and the extended minimum around phase 0.5 are well reproduced. The time modulation is caused by the observer’s changing projected surface area of overdense $H\alpha$ emitting wind plasma as the star rotates. At maximum emission (phase 0), the DM is viewed essentially from above the magnetic pole, whereas at minimum (phase 0.5) it is viewed almost edge-on. Thus the DM in the latter phase has a smaller projected surface area, leading to weaker emission.

The good overall agreement between observations and simulations obtained for HD 191612 is encouraging, and provides strong support for the basic concept of the dynamical magnetosphere model. We are currently in the process of extending the modeling presented here to more magnetic O stars with $R_\star < R_A < R_K$ that also show periodic Balmer emission, like HD 57682 (Grunhut et al., submitted to MNRAS) and θ^1 Ori C.

Acknowledgments. J.O.S. gratefully acknowledges funding from NASA ATP grant NNX11AC40G

References

- Bouret, J.-C., Lanz, T., Hillier, D. J., Heap, S. R., Hubeny, I., Lennon, D. J., Smith, L. J., & Evans, C. J. 2003, *ApJ*, 595, 1182. [arXiv:astro-ph/0301454](#)
- Castor, J. I., Abbott, D. C., & Klein, R. I. 1975, *ApJ*, 195, 157
- Cohen, D. H., Gagné, M., Leutenegger, M. A., MacArthur, J. P., Wollman, E. E., Sundqvist, J. O., Fullerton, A. W., & Owocki, S. P. 2011, *ArXiv e-prints*. 1104.4786
- Cohen, D. H., Leutenegger, M. A., & Townsend, R. H. D. 2008, in *Clumping in Hot-Star Winds*, edited by W.-R. Hamann, A. Feldmeier, & L. M. Oskinova, 209. 0712.1050
- Cohen, D. H., Leutenegger, M. A., Wollman, E. E., Zsargó, J., Hillier, D. J., Townsend, R. H. D., & Owocki, S. P. 2010, *MNRAS*, 405, 2391. 1003.0892
- Dessart, L., & Owocki, S. P. 2005, *A&A*, 437, 657. [arXiv:astro-ph/0503514](#)
- Eversberg, T., Lepine, S., & Moffat, A. F. J. 1998, *ApJ*, 494, 799
- Feldmeier, A. 1995, *A&A*, 299, 523
- Feldmeier, A., Oskinova, L., & Hamann, W.-R. 2003, *A&A*, 403, 217. [arXiv:astro-ph/0302516](#)
- Feldmeier, A., Puls, J., & Pauldrach, A. W. A. 1997, *A&A*, 322, 878
- Fullerton, A. W., Massa, D. L., & Prinja, R. K. 2006, *ApJ*, 637, 1025. [arXiv:astro-ph/0510252](#)
- Howarth, I. D., Walborn, N. R., Lennon, D. J., Puls, J., Nazé, Y., Annuk, K., Antokhin, I., Bohlender, D., & Bond, H. . 2007, *MNRAS*, 381, 433. 0707.0594
- Lucy, L. B. 1984, *ApJ*, 284, 351
- Markova, N., Puls, J., Scuderi, S., & Markov, H. 2005, *A&A*, 440, 1133. [arXiv:astro-ph/0505613](#)
- Muijres, L. E., de Koter, A., Vink, J. S., Krtićka, J., Kubát, J., & Langer, N. 2011, *A&A*, 526, A32
- Najarro, F., Hanson, M. M., & Puls, J. 2011, *ArXiv e-prints*. 1108.5752
- Oskinova, L. M., Feldmeier, A., & Hamann, W.-R. 2006, *MNRAS*, 372, 313. [arXiv:astro-ph/0603286](#)
- Oskinova, L. M., Hamann, W.-R., & Feldmeier, A. 2007, *A&A*, 476, 1331. 0704.2390
- Owocki, S. P. 2008, in *Clumping in Hot-Star Winds*, edited by W.-R. Hamann, A. Feldmeier, & L. M. Oskinova, 121
- Owocki, S. P., Castor, J. I., & Rybicki, G. B. 1988, *ApJ*, 335, 914
- Owocki, S. P., & Cohen, D. H. 2006, *ApJ*, 648, 565. [arXiv:astro-ph/0602054](#)
- Owocki, S. P., Gayley, K. G., & Shaviv, N. J. 2004, *ApJ*, 616, 525. [arXiv:astro-ph/0409573](#)
- Owocki, S. P., & Puls, J. 1996, *ApJ*, 462, 894
- Owocki, S. P., & Rybicki, G. B. 1984, *ApJ*, 284, 337
- 1985, *ApJ*, 299, 265
- Puls, J., Markova, N., Scuderi, S., Stanghellini, C., Taranova, O. G., Burnley, A. W., & Howarth, I. D. 2006, *A&A*, 454, 625. [arXiv:astro-ph/0604372](#)
- Puls, J., Urbaneja, M. A., Venero, R., Repolust, T., Springmann, U., Jokuthy, A., & Mokiem, M. R. 2005, *A&A*, 435, 669. [arXiv:astro-ph/0411398](#)
- Puls, J., Vink, J. S., & Najarro, F. 2008, *A&A Rev.*, 16, 209. 0811.0487

- Sundqvist, J. O., Owocki, S. P., Cohen, D. H., Leutenegger, M. A., & Townsend, R. H. D. 2012a, MNRAS, 420, 1553. 1111.1762
- Sundqvist, J. O., Owocki, S. P., & Puls, J. 2011a, ArXiv e-prints. 1110.0485
- Sundqvist, J. O., Puls, J., & Feldmeier, A. 2010, A&A, 510, A11+. 0911.3361
- Sundqvist, J. O., Puls, J., Feldmeier, A., & Owocki, S. P. 2011b, A&A, 528, A64+. 1101.5293
- Sundqvist, J. O., ud-Doula, A., Owocki, S. P., Townsend, R. H. D., Howarth, I. D., & Wade, G. A. 2012b, MNRAS, L433. 1203.1050
- Townsend, R. H. D., & Owocki, S. P. 2005, MNRAS, 357, 251. arXiv:astro-ph/0408565
- ud-Doula, A., & Owocki, S. P. 2002, ApJ, 576, 413
- ud-Doula, A., Owocki, S. P., & Townsend, R. H. D. 2008, MNRAS, 385, 97. 0712.2780
- Vink, J. S., de Koter, A., & Lamers, H. J. G. L. M. 2000, A&A, 362, 295. arXiv:astro-ph/0008183
- Wade, G. A., Howarth, I. D., Townsend, R. H. D., Grunhut, J. H., Shultz, M., Bouret, J.-C., Fullerton, A., Marcolino, W., Martins, F., Nazé, Y., Ud Doula, A., Walborn, N. R., & Donati, J.-F. 2011, MNRAS, 416, 3160. 1106.3008